electronics

MDPI

Article

Modeling and Simulation of Wide-Frequency Characteristics of Electromagnetic Standard Voltage Transformer

Lewei Wang [1,*], Zhenhua Li [1,2], Heping Lu [3], Feng Zhou [3] and Yinglong Diao [3]

[1] School of Electrical Engineering and New Energy, China Three Gorges University, Yichang 443002, China; lizhenhua1993@163.com
[2] Provincial Engineering Research Center of Intelligent Energy Technology, China Three Gorges University, Yichang 443002, China
[3] China Electric Power Research Institute, Wuhan 430074, China; lhp@epri.sgcc.com.cn (H.L.); zhoufeng@epri.sgcc.com.cn (F.Z.); diaoyinglong@126.com (Y.D.)
* Correspondence: wanglewei381@gmail.com

Abstract: To achieve the broadband applicability of standard voltage transformers in "dual high" power systems, an equivalent circuit model of the standard voltage transformer is first established. Using the complex magnetic permeability method and utilizing existing core parameters, the excitation impedance values are obtained. Next, based on the equivalent circuit model, the no-load error function of the standard voltage transformer is analyzed, and through simulation, the no-load error response curve of the standard voltage transformer in the frequency range of 20 Hz to 3000 Hz is derived. The simulation results indicate that within the 20 Hz to 700 Hz range, both the no-load ratio error and the no-load angular error meet the accuracy requirements, with the ratio error within ±0.05% and the angular error within 2′. Additionally, the derivation of the error transfer function demonstrates the correlation between the no-load error values and the number of turns and cross-sectional area of the standard voltage transformer. Simulation results, obtained by increasing and decreasing the number of turns and cross-sectional area by 10%, provide valuable insights for the error compensation and structural design of standard voltage transformers.

Keywords: standard voltage transformer; wide frequency; complex permeability; excitation impedance; no-load error

check for updates

Citation: Wang, L.; Li, Z.; Lu, H.; Zhou, F.; Diao, Y. Modeling and Simulation of Wide-Frequency Characteristics of Electromagnetic Standard Voltage Transformer. *Electronics* **2024**, *13*, 4206. https://doi.org/10.3390/electronics13214206

Academic Editor: Jahangir Hossain

Received: 23 September 2024
Revised: 24 October 2024
Accepted: 25 October 2024
Published: 27 October 2024

Copyright: © 2024 by the authors. Licensee MDPI, Basel, Switzerland. This article is an open access article distributed under the terms and conditions of the Creative Commons Attribution (CC BY) license (https://creativecommons.org/licenses/by/4.0/).

1. Introduction

With the rapid development of the global economy and industry, energy demand continues to rise, and large-scale renewable energy is being integrated into power grids via power electronic devices. It is projected that by 2050, renewable energy will account for 55% of global electricity generation [1], while in China, this figure is expected to exceed 85% [2]. Meanwhile, the application of flexible AC/DC transmission technology and the re-electrification of the load side are driving the widespread use of power electronic devices in power transmission and on the user end. In summary, the rapid development of renewable energy sources such as wind and solar, along with the transformation of core equipment in the source–grid–load chain toward "power electronics," is pushing the power system toward a trend of "high renewable energy penetration" and "high power electronics penetration" (referred to as the "dual high" trend) [3].

In the "dual high" power system, the key characteristics of the grid have undergone significant changes, exhibiting multimodal and time-varying features. Besides the power frequency signal, the voltage in the power system also includes transient signals in the low to medium and medium to high frequency ranges, as well as high-frequency transient signals. These signals can arise from various factors such as ferromagnetic resonance and load switching, which generate low to medium frequency signals, while medium to high frequency and high-frequency transients can be caused by events like line reclosing,

short-circuit faults, lightning strikes, and gas-insulated substation faults. Additionally, renewable energy units or converters can induce electromagnetic resonance across a wide frequency range, from 0 Hz to several hundred Hz. The traditional standard voltage transformer, which is limited to measuring power frequency voltage signals, is unable to meet the real-time voltage sensing requirements across such a wide range of frequencies and bandwidths [4–7].

A voltage transformer, in principle, is a type of transformer used to transmit corresponding voltage signals to measurement instruments. In the power market, its primary application is in energy metering, where its accuracy directly affects the fairness and equity of energy transactions. The standard voltage transformer, on the other hand, is used for the calibration and analysis of measured transformers to ensure that errors are controlled within the specified accuracy range [8–10].

The standard voltage transformer is one of the most widely used voltage transformers, designed based on the law of electromagnetic induction. Error is a key metric for evaluating its performance, with sources of error related to the excitation characteristics of ferromagnetic materials and the structure of the device. During the repeated magnetization process of ferromagnetic materials under alternating magnetic fields, magnetic domains continuously rotate and interact, leading to hysteresis loss. This hysteresis loss represents the instantaneous power required for the core to establish alternating magnetic flux and overcome domain rotation, which is frequency dependent. When the frequency changes, the variation in hysteresis loss inevitably affects the hysteresis loop, thus altering the excitation characteristics of the core [11–13].

Currently, research on standard voltage transformers primarily focuses on the traceability of the devices and error accuracy across different voltage levels. However, studies on the performance of standard voltage transformers under wide frequency ranges remain limited, and there is still a need to enhance and refine experimental testing and calibration within the 20 Hz to 3000 Hz frequency range.

Papers [14–16] analyze the high- and low-voltage test circuits and transfer functions of standard voltage transformers, simulate their performance across different voltage levels, and conduct comparative validations of the results. However, these studies do not address the frequency characteristics of standard voltage transformers.

The paper [17,18] presents the equivalent circuit model of the standard voltage transformer, analyzes its excitation impedance, and introduces calculation and measurement methods for the primary and secondary sides, including the resistances and inductances. The no-load error curves at 20 Hz and 50 Hz are obtained through simulation, providing support for the use of standard voltage transformers in low-frequency flexible AC transmission systems. However, further research is still needed to evaluate the applicability of standard voltage transformers across a wider frequency range.

Therefore, research on the broadband characteristics of standard voltage transformers within the 20 Hz to 3000 Hz range has become indispensable.

This paper will use a 10 kV standard voltage transformer as a model, to measure its circuit parameters and analyze the theoretical and actual errors of the transformer in the 20 Hz to 3 kHz range. The corresponding error frequency characteristics will be derived, providing theoretical support for the application of standard voltage transformers in broadband scenarios.

2. Development of an Error Model for Standard Voltage Transformers

In the absence of core magnetic saturation, the main flux and leakage flux in a standard voltage transformer vary sinusoidally with time t at the frequency f of the source voltage. According to Faraday's law of electromagnetic induction, the instantaneous value of the induced electromotive force in the winding due to the main flux is:

$$e_1 = -N\frac{d\Phi_m \sin \omega t}{dt} = -j2\pi f N \Phi_m \cos \omega t \quad (1)$$

The effective value E of the induced electromotive force is related to the peak value Φ_m of the main flux by:

$$E = \sqrt{2}\pi f N \Phi_m = \sqrt{2}\pi f N B_m S \quad (2)$$

Under the assumption that leakage flux and winding resistance drops are negligible, it is considered that $u_1 \approx e_1$ and $U_1 \approx E$, where U_1 represents the effective value of the supply voltage. Given that the mutual transformer structural parameters (S,N) remain constant, B_m is inversely proportional to the frequency f when U_1 is constant. Therefore, as the frequency f decreases, the core magnetic flux density increases. The rated working magnetic flux density of the core in standard voltage transformers is often greater than 1.0 T, and it may reach saturation as the frequency f decreases. To maintain a constant core magnetic flux density, it is necessary to increase the core cross-sectional area S or the number of winding turns N when the frequency f decreases.

The most commonly used structure for electromagnetic standard voltage transformers is the SF6 gas-insulated type. The core is assembled from laminated silicon steel sheets, followed by winding the secondary and primary windings in sequence. A high-voltage shielding cover is then added, and the high-voltage lead is routed through a post insulator. The primary winding adopts a tower-shaped, single-stage trapezoidal structure. The equivalent circuit model of the standard voltage transformer is shown in Figure 1.

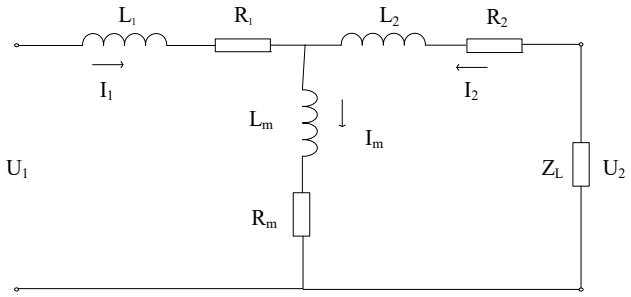


Figure 1. Equivalent circuit model of standard voltage transformer.

In Figure 1, L_1 and R_1 are the primary winding leakage inductance and DC resistance, L_m and R_m are the excitation inductance and excitation resistance, L_2 and R_2 are the secondary winding leakage inductance and DC resistance (converted to the primary side), Z_L is the standard voltage transformer load (converted to the primary side), U_1 is the primary voltage, and U_2 is the secondary voltage (converted to the primary side).

For the standard voltage transformer that has been designed, L_1, L_2, R_1, R_2 are constant, Z_L includes resistance and inductance, the value of which is only related to the size of the load, and none of the above parameters are affected by frequency. While R_m corresponds to the equivalent resistance of the iron core loss, L_m is a parameter that characterizes the magnetization performance of the iron core, which is affected by the excitation characteristics of the ferromagnetic material; R_m and L_m are not constant but vary with the degree of iron core saturation. For obtaining the wide-frequency equivalent circuit element parameters of the standard voltage transformer, the acquisition of the wide-frequency parameters of the excitation impedance is particularly important [19,20].

3. Frequency Characteristics of Complex Permeability of Ferromagnetic Materials

When analyzing the harmonic characteristics of electromagnetic transformers, the influence of the distribution capacitance is often considered, while ignoring the variation in the excitation impedance with frequency. For the high precision standard voltage transformer with wide frequency, it is necessary to consider the frequency characteristics of the excitation impedance [21–23]. The nonlinearity of the excitation impedance is mainly affected by the excitation characteristics of ferromagnetic materials, including two parameters: one is the permeability, representing the ability of ferromagnetic materials to conduct magnetic flux, often used to express the real permeability μ, which is defined as

the magnetic flux density B to the ratio of the magnetic field strength H, usually extracted from the DC magnetization curve; the other is the core loss angle, representing the AC excitation, due to the influence of ferromagnetic loss; the magnetic induction strength B lags behind the magnetic field strength H by a phase angle, denoted by θ. Considering that there is an angular difference between H and B under AC excitation, H and B can be expressed by Equations (3) and (4).

$$H = H_m \sin \omega t \tag{3}$$

$$B = B_m \sin(\omega t - \theta) \tag{4}$$

H_m is the magnitude of the magnetic field strength; B_m is the magnitude of the magnetic flux density.

The complex permeability of a ferromagnetic material in one cycle can be expressed as:

$$\mu = \frac{B}{H} = \frac{B_m}{H_m} e^{-j\theta} = \mu' - j\mu'' \tag{5}$$

The real and imaginary parts of the complex permeability are, respectively:

$$\mu' = \frac{B_m \cos \theta}{H_m} \tag{6}$$

$$\mu'' = \frac{B_m \sin \theta}{H_m} \tag{7}$$

The core loss angle tangent is:

$$\mathrm{tg}\theta = \frac{\mu''}{\mu'} \tag{8}$$

The current electromagnetic transformer core is a laminated structure, whose thickness is much less than the width and length, so only the one-dimensional flow of current is considered [24–26]; H_Z represents the magnetic field intensity applied in the z-direction, which leads to the following equation:

$$\frac{\partial^2 H_Z}{\partial x^2} = \mu_0 \mu_r (j\omega\sigma - \omega^2 \varepsilon) H_z = k^2 H_Z \tag{9}$$

where k is the propagation constant, calculated as:

$$k = (1 + j)\sqrt{\frac{\omega \sigma \mu_0 \mu_r}{2}} \tag{10}$$

b is the thickness of the silicon steel sheet; ω is the excitation signal angular frequency; σ is the core conductivity; μ_0 is the vacuum permeability; $\mu_0 = 4\pi \times 10^{-7}$ H/m; and μ_r is the relative permeability.

Then, the magnetic field strength at the surface of the core is calculated as:

$$H = \frac{k\Phi}{2\mu_0 \mu_r h} \mathrm{cotan}h(k\frac{b}{2}) \tag{11}$$

where H denotes the magnetic field strength at the surface of the core; the width of the stack is h; and Φ denotes the magnetic flux through a cross-sectional area of bh. Therefore, the space-averaged magnetic flux density B in the z-direction is related to the magnetic flux through the cross-sectional area; i.e.,

$$\overline{B} = \frac{k_{Fe}\Phi}{bh} \tag{12}$$

k_{Fe} is the core stacking factor, $k_{Fe} = b/(b + \Delta)$. The complex permeability of the core stack is the ratio of the spatially averaged magnetic flux density to the surface magnetic field strength H; i.e.,

$$\mu = \frac{\overline{B}}{H} = k_{Fe}\mu_r \frac{\tan h(\frac{kb}{2})}{\frac{kb}{2}} \tag{13}$$

μ_i is the initial magnetic permeability, where Δ is the thickness of the insulation layer. Where the model relative permeability μ_r is close to the initial permeability μ_i of the core, μ_i is defined as the relative permeability at zero magnetic field strength; i.e.,

$$\mu_r \approx \mu_i = \frac{1}{\mu_0} \lim_{H \to 0} \frac{B}{H} \tag{14}$$

$$\mu = \frac{\overline{B}}{H} = k_{Fe}\mu_i \frac{\tan h(\frac{kb}{2})}{\frac{kb}{2}} \tag{15}$$

According to the simulation model, the relative complex permeability of the silicon steel sheet's real part μ', imaginary part μ'', amplitude $\mid \mu \mid$ and the core loss angle θ by the frequency influence curve, and hysteresis loop measurement of the curve is compared with the curve shown in Figure 2; the simulation model used in the specific parameters is shown in Table 1.

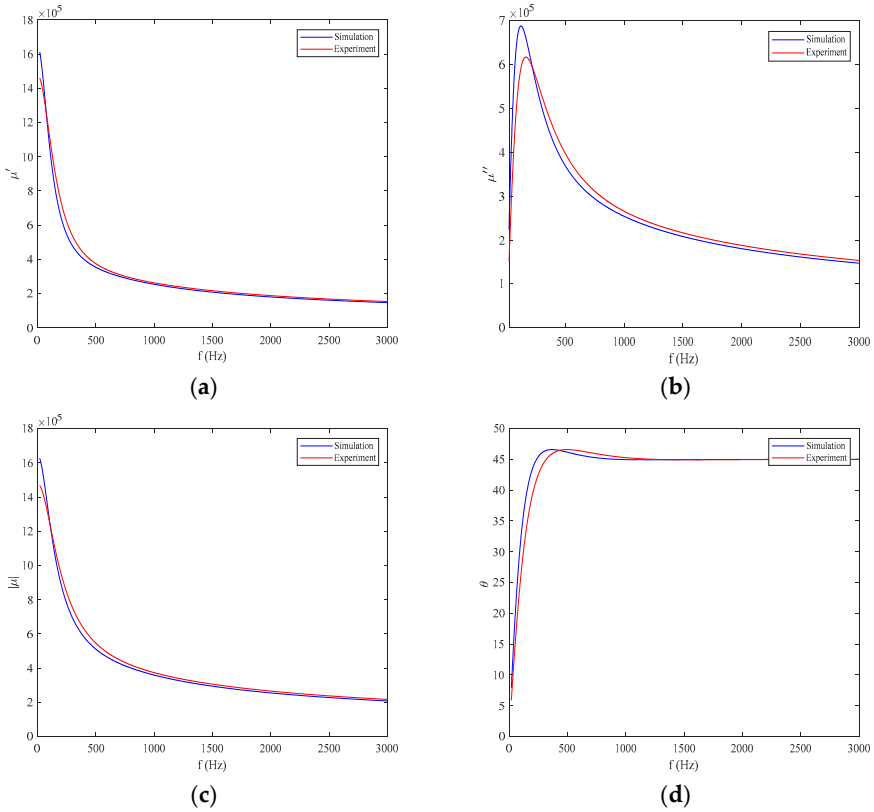


Figure 2. Frequency response curves for 4 parameters. (**a**) $\mu' - f$ frequency response curve; (**b**) $\mu'' - f$ frequency response curve; (**c**) $\mid \mu \mid - f$ frequency response curve; (**d**) $\theta - f$ frequency response curve.

Table 1. Iron core parameters.

Symbol	Quantity	Numerical Value
b	core thickness	0.0625/m
Δ	insulation thickness	1.5/mm
ρ	core resistivity	$1.29 \times 10^{-6}/(\Omega \cdot m)$
σ	core conductivity	$7.7 \times 10^{5}/(S \cdot m^{-1})$
μ_i	relative permeability of core	$1.7 \times 10^{6}/H \cdot m^{-1}$
N_1	primary measured winding turns	9000
l_1	flux path length	0.78/m
d_1	thickness of primary side winding	0.62/mm
d_2	secondary measured winding thickness	13.58/mm
h	winding height	620/mm
p	the average turn length	100/mm
μ_0	vacuum permeability	$1.26 \times 10^{-6}/(H \cdot m^{-1})$

Four situations are analyzed in detail as follows:

(a) $\mu' - f$ frequency response curve;
(b) $\mu'' - f$ frequency response curve;
(c) $\mid \mu \mid -f$ frequency response curve;
(d) $\theta - f$ frequency response curve.

From the simulation results in Figure 2, the relative complex permeability real part μ', imaginary part μ'', magnitude $\mid \mu \mid$, and core loss angle θ are basically the same as the curve model derived from the hysteresis loop measurements, which verifies the feasibility of calculating the complex permeability of the iron core through the structural parameters, and provides the corresponding parameter support for the subsequent simulation model of the transformer error.

4. No-Load Error Frequency Characterization of Standard Voltage Transformers

The errors in standard voltage transformers include ratio errors and phase errors. The ratio error refers to the discrepancy caused by the difference between the actual transformation ratio and the rated transformation ratio during measurement. Angular difference is between the primary and secondary voltage phases [27,28].

According to the standard voltage transformer equivalent circuit diagram shown in Figure 1, the difference between its secondary voltage and primary voltage can be written as:

$$\Delta U(\omega) = U_2'(\omega) - U_1(\omega) = -I_2'(\omega)(Z_1(\omega) + Z_2(\omega)) - I_m(\omega)Z_m(\omega) \tag{16}$$

Then, the error of the standard voltage transformer is:

$$\frac{\Delta U(\omega)}{U_1'(\omega)} = -\frac{Z_1(\omega)}{Z_1(\omega) + Z_m(\omega)} - \frac{Z_1(\omega) + Z_2'(\omega)}{Z_1(\omega) + Z_2'(\omega) + Z_L'(\omega)} \tag{17}$$

According to the definition of transformer error, the equations for the no-load ratio error and angular error are, respectively:

$$\varepsilon_0(\omega) = \left|\frac{U_2'(\omega)}{U_1(\omega)}\right| - 1 = \left|\frac{Z_m(\omega)}{Z_m(\omega) + Z_l(\omega)}\right| - 1 \tag{18}$$

$$\delta_0(\omega) = \angle U_1(\omega) - \angle U_2'(\omega) = \angle(Z_1(\omega) + Z_m(\omega)) - \angle Z_m(\omega) \tag{19}$$

The standard voltage transformer is an electromagnetic voltage ratio standard, typically operated with no load or nearly zero load on the secondary side. Therefore, this paper focuses on discussing the no-load error characteristics of the standard voltage transformer.

In this paper we consider a 10 kV standard voltage transformer as the specimen, with a rated voltage of 10/0.1 kV. The iron core material is a silicon steel sheet B30P105, with a

cross-sectional area of S = 50 cm^2, an average magnetic path length of 78 cm, and a turns ratio of 9000/90. Firstly, the leakage inductance and DC resistance of the primary winding of the transformer are calculated based on the structural parameters.

When a direct current (DC) flows through the coil, the resulting losses can be considered as DC losses. The corresponding DC resistance is determined by the material and geometric structure of the coil [29,30], and can be calculated using Equation (20).

$$R_1 = \frac{\rho l_1}{S} \tag{20}$$

In the equation, R_1 represents the DC resistance of the coil, ρ denotes the resistivity of the conductor, l_1 is the length of the primary winding conductor, and S represents the cross-sectional area of the conductor.

In practical design, the leakage inductance of the primary winding of a transformer can be estimated using an analytical method, with the calculation equation given by Equation (21):

$$L1 = \frac{\mu_0 N_1^2 p}{h}(\Delta + \frac{d_1 + d_2}{3}) \tag{21}$$

In the equation, N_1 represents the number of turns in the primary winding, p denotes the average turn length of the winding, h is the height of the winding, Δ, d_1, and d_2 represent the insulation thickness between the primary and secondary windings, the thickness of the primary winding, and the thickness of the secondary winding, respectively.

The error equations for the standard voltage transformer are given by Equations (18) and (19). Therefore, by obtaining the parameters of the excitation impedance, we can calculate the ratio error and angular angle error of the standard voltage transformer.

In the calculation of transformer parameters, the value of excitation impedance is related to the real and imaginary parts of the complex magnetic permeability, as shown in Equations (22) and (23).

$$L_m = \frac{N_1^2 \mu' S}{l} \tag{22}$$

$$R_m = \frac{\omega N_1^2 \mu'' S}{l} \tag{23}$$

After calculation, the values of excitation impedance at frequencies ranging from 20 Hz to 3000 Hz are obtained, and the frequency response curve of the excitation impedance is plotted as shown in Figure 3.

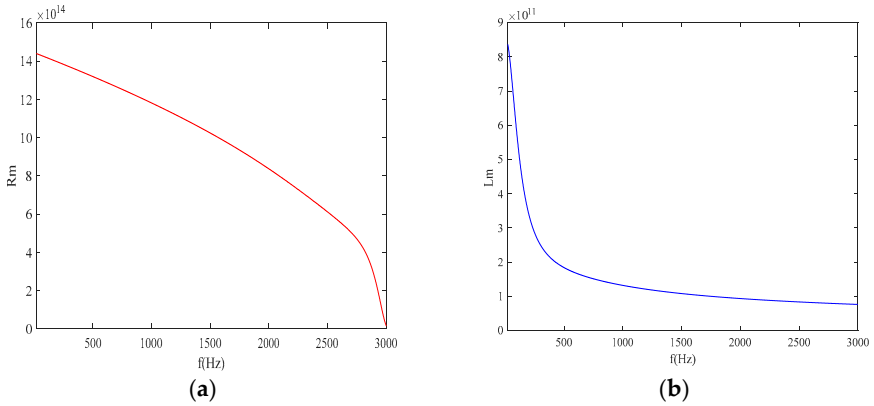


Figure 3. Excitation impedance frequency response curves. (**a**) $R_m - f$ frequency response curve; (**b**) $L_m - f$ frequency response curve.

As the frequency increases, the eddy current effect enhances, resulting in a decrease in the excitation inductance in the transformer coil. Additionally, at wide frequency ranges, the rate of decrease in the imaginary part of the complex magnetic permeability exceeds

the rate of increase in frequency. Consequently, the excitation impedance decreases with the increase in frequency.

According to R_1, $L1$, R_m, and L_m, the corresponding equation, brought to Equations (18) and (19), can be calculated in the standard voltage transformer in the 20 Hz to 3000 Hz range, under the ratio of the angle difference; the simulation calculation results are shown in Table 2.

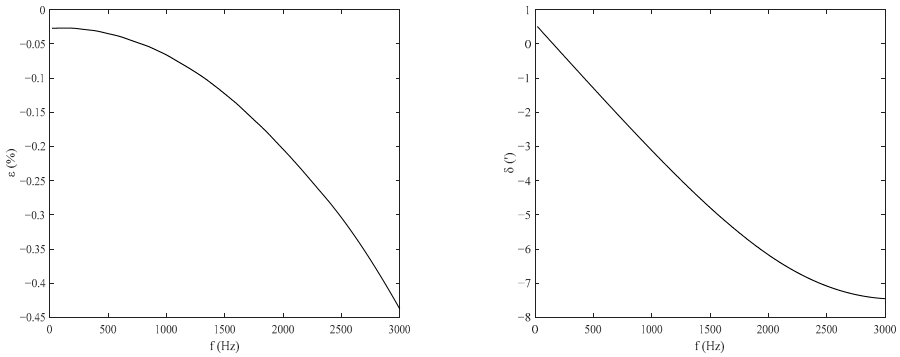
Table 2. Calculated values of ratio difference and angle difference at 20 Hz to 3000 Hz.

Frequency	ε_0	δ_0	Frequency	ε_0	δ_0
/Hz	/(%)	/(′)	/Hz	/(%)	/(′)
20	−0.023	0.507	1450	−0.110	−4.628
30	−0.023	0.471	1500	−0.116	−4.785
40	−0.023	0.433	1550	−0.123	−4.939
50	−0.024	0.396	1600	−0.130	−5.091
100	−0.024	0.207	1650	−0.137	−5.235
150	−0.025	0.018	1700	−0.145	−5.382
200	−0.026	−0.169	1750	−0.153	−5.523
250	−0.027	−0.367	1800	−0.161	−5.662
300	−0.028	−0.545	1850	−0.169	−5.791
350	−0.029	−0.732	1900	−0.177	−5.923
400	−0.030	−0.919	1950	−0.186	−6.045
450	−0.031	−1.105	2000	−0.195	−6.165
500	−0.033	−1.291	2050	−0.204	−6.282
550	−0.035	−1.477	2100	−0.213	−6.391
600	−0.037	−1.662	2150	−0.223	−6.495
650	−0.039	−1.847	2200	−0.232	−6.595
700	−0.042	−1.997	2250	−0.242	−6.691
750	−0.045	−2.213	2300	−0.252	−6.775
800	−0.048	−2.395	2350	−0.262	−6.866
850	−0.051	−2.576	2400	−0.272	−6.942
900	−0.054	−2.756	2450	−0.282	−7.011
950	−0.058	−2.935	2500	−0.293	−7.075
1000	−0.062	−3.112	2550	−0.303	−7.135
1050	−0.066	−3.288	2600	−0.314	−7.191
1100	−0.071	−3.462	2650	−0.325	−7.242
1150	−0.076	−3.635	2700	−0.337	−7.289
1200	−0.081	−3.806	2750	−0.349	−7.331
1250	−0.086	−3.975	2800	−0.363	−7.368
1300	−0.092	−4.142	2850	−0.377	−7.399
1350	−0.097	−4.306	2900	−0.407	−7.424
1400	−0.103	−4.469	3000	−0.436	−7.459

Based on the simulation values, the frequency response curves of the standard voltage transformer ratio difference and angular difference at 20–3000 Hz can be plotted, as shown in Figure 4.

According to the national standards, for the 10 kV electromagnetic standard voltage transformer studied in this paper, during normal operation, the ratio difference should be within ±0.05%, and the angular difference should be within 2′.

Based on the analysis of Figure 4, it is evident that when the frequency of the standard voltage transformer is between 20 Hz and 700 Hz, the ratio error remains within ±0.05%, and the angular error is within 2 min, indicating accurate measurement results. At 700 Hz, the ratio error is −0.042%, and the angular error is −1.997′. However, when the frequency exceeds 700 Hz, the ratio and angular errors no longer meet the required accuracy, demonstrating that the standard voltage transformer cannot provide accurate measurements for high-frequency voltages. Additionally, according to the error calculation equation, the design of the standard voltage transformer can be optimized by compensating the number of turns or altering the cross-sectional area to obtain a more favorable error curve.

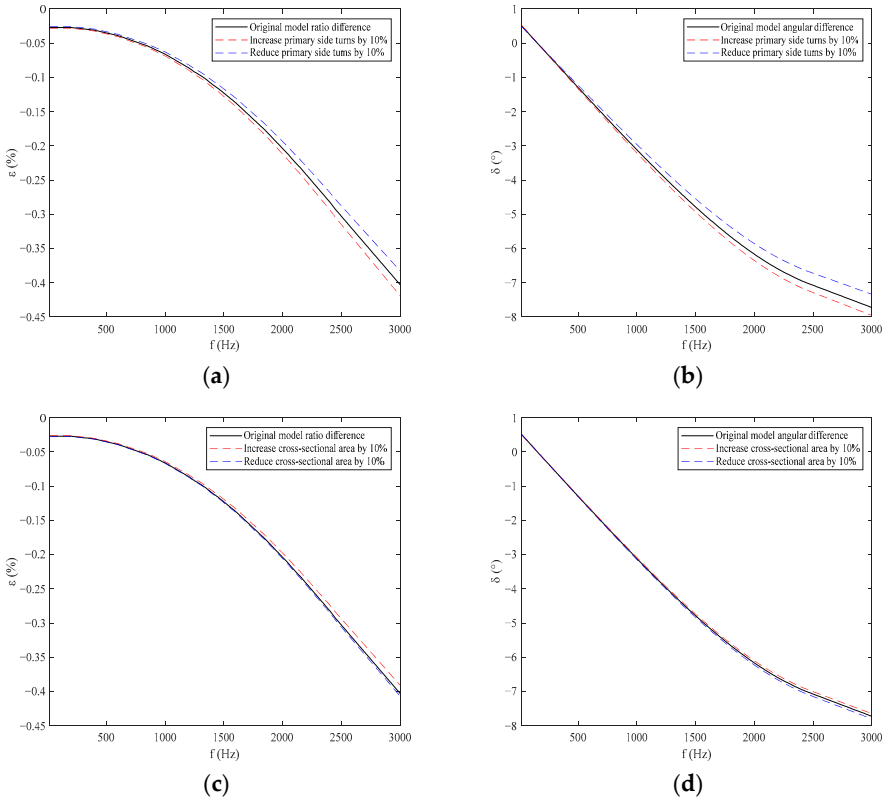


(**a**) (**b**)

Figure 4. Error response curve of standard voltage transformer at 20 Hz to 3000 Hz. (**a**) Ratio difference frequency response curve; (**b**) angular difference frequency response curve.

5. The Impact of Altering Core Parameters on the Frequency Characteristics of No-Load Error

In actual operating conditions, variations in parameters may occur due to differences in manufacturing methods, winding processes, and materials used for standard voltage transformers. Analysis of Equations (18)–(23) reveals that the number of turns and cross-sectional area of the standard voltage transformer can affect the no-load error. To investigate the impact of changing these parameters on the ratio error and angular error, simulations were conducted. The simulation results are presented in Figure 5.



(**a**) (**b**)

(**c**) (**d**)

Figure 5. Frequency response curve of the error corresponding to changing N1 and S. (**a**) Effect of changing N_1 on ratio difference; (**b**) effect of changing N_1 on angular difference; (**c**) effect of changing the S on ratio difference; (**d**) effect of changing the S on angular difference.

Based on the simulation results shown in Figure 5, it is observed that reducing the number of turns in the primary winding (N_1) decreases both the no-load ratio difference and

angular error of the standard voltage transformer within the 20 Hz to 3000 Hz frequency range, with the changes being particularly significant. Increasing the core cross-sectional area (S) also reduces the no-load ratio difference over the same frequency range, while the angular error exhibits minimal variation. However, a reduction in angular error becomes noticeable when the frequency exceeds 1000 Hz. Therefore, in the design of standard voltage transformers, appropriately reducing the number of turns in the primary winding or increasing the core cross-sectional area can enhance the transformer's performance across a wide frequency range.

6. Conclusions

1. The complex permeability can characterize the magnetization of silicon steel sheets in a varying magnetic field. Based on the corresponding equations, the frequency response curves of the real and imaginary parts of the complex permeability, as well as the core loss angle, were plotted. These results are consistent with conclusions drawn from hysteresis loop measurements, providing the necessary parameter support for further research into the frequency characteristics of the excitation impedance of standard voltage transformers.
2. The no-load error of a standard voltage transformer is related to the primary leakage reactance and excitation impedance. The primary leakage reactance can be determined based on the structural parameters of the transformer, while the excitation impedance is associated with the complex permeability. By calculating the excitation impedance using the relevant equations and simulating the frequency response curve of the excitation impedance, the process of obtaining the no-load error values for the transformer within the 20–3000 Hz frequency range is facilitated.
3. The no-load error of a standard voltage transformer can be divided into ratio error and angular error. Calculation results show that within the frequency range of 20 Hz to 700 Hz, the influence of the ratio error is less than 0.05%, and the influence of the angular error is less than 2′. Based on the error limit values for voltage transformers used in measurement, it can be concluded that by fully considering the effects of core magnetic flux density and frequency during design, the no-load error of standard voltage transformers can meet the requirements of 0.05 class or lower error limits within the 20 Hz to 700 Hz range, but when the frequency exceeds 700 Hz, the error accuracy will not meet the requirements, so in order to realize a standard voltage transformer which can meet the error limit at a wide range of frequencies, further experiments and simulations are required.
4. The derivation of the error equation shows the correlation between the no-load error value of the standard voltage transformer and the number of turns of the iron core, as well as the cross-sectional area, and the simulation results show that reducing the number of turns of the primary winding or increasing the cross-sectional area of the iron core will reduce the error value; this conclusion provides a corresponding support for the design of the standard voltage transformer under broadband frequencies, and provides a certain reference for the manufacturers in the design of standard voltage transformers for civilian use; and, at the same time, the influence of the error factors are discussed, and the proposed number of turns and cross-sectional area for the study of other types of voltage transformer errors provide a corresponding value.

Author Contributions: Conceptualization, L.W. and Z.L.; methodology, L.W. and Z.L.; software, L.W. and H.L.; validation, L.W. and H.L.; investigation, L.W. and F.Z.; writing—original draft preparation, L.W.; writing—review and editing, L.W. and F.Z.; project administration, Y.D.; funding acquisition, Y.D. All authors have read and agreed to the published version of the manuscript.

Funding: This work was supported in part by the National Key R&D Program of China (2022YFB2403800) Key Technologies of Multi-Parameter Wide-Area Sensing and Measurement for Massive Electricity Users, and in part by the National Natural Science Foundation of China (52277012).

Data Availability Statement: Data are contained within the article.

Acknowledgments: The authors would like to thank all reviewers for their helpful comments and suggestions regarding this paper.

Conflicts of Interest: Author Heping Lu, Feng Zhou and Yinglong Diao were employed by the company China Electric Power Research Institute. The remaining authors declare that the research was conducted in the absence of any commercial or financial relationships that could be construed as a potential conflict of interest.

References

1. Peng, Y.; Feng, L.; Qirong, J.; Hangyin, M. Large-disturbance stability of power systems with high penetration of renewables and inverters: Phenomena, challenges, and perspectives. *J. Tsinghua Univ. (Sci. Technol.)* **2021**, *61*, 403–414.
2. Hu, J.; Yuan, X.; Cheng, S. Multi-time scale transients in power-electricized power systems considering multi-time scale switching control schemes of power electronics apparatus. *Proc. CSEE* **2019**, *39*, 5457–5467.
3. Yuan, X.; Cheng, S.; Hu, J. Multi-time scale voltage and power angle dynamics in power electronics dominated large power systems. *Proc. CSEE* **2016**, *36*, 5145–5154.
4. Xie, X.; He, J.; Mao, H.; Li, H. New issues and classification of power system stability with high shares of renewables and power electronics. *Proc. CSEE* **2021**, *41*, 461–475.
5. Ding, J. Research on Broadband Measurement Performance of Power Transformer. Master's Thesis, China Electric Power Research Institute, Beijing, China, 2020.
6. Yao, M.; Liao, S.; Lin, F.; Long, Z.; Liu, R.; Liu, Y. Overview of broadband measurement characteristics of voltage sensing devices. In Proceedings of the 2024 IEEE 7th International Electrical and Energy Conference (CIEEC), Harbin, China, 10–12 May 2024; pp. 3238–3245.
7. Zhang, Z.; Lu, H.; Li, B.; Ding, L. Research on data-driven self-diagnosis for measurement errors in capacitor voltage Transformers. *IEEE Trans. Instrum. Meas.* **2024**, *73*, 3524712. [CrossRef]
8. Frljić, S.; Trkulja, B.; Drandić, A. Eddy current losses in power voltage transformer open-type cores. *COMPEL-Int. J. Comput. Math. Electr. Electron. Eng.* **2023**, *42*, 1039–1051. [CrossRef]
9. Akhmeev, A.; Voronskaya, E. Measuring installation for the research of errors of measuring current transformers in the extended frequency range 40–2500 Hz. *Meas. Tech.* **2023**, *66*, 119–123. [CrossRef]
10. Zhou, G.; Chen, X.; Zheng, H.; Yin, J.; Peng, C. Wide-frequency range voltage monitoring device for current transformer. *J. Phys. Conf. Ser.* **2023**, *2450*, 012004. [CrossRef]
11. Van Niekerk, D.; Schoombie, B.; Bokoro, P. Design of an experimental approach for characterization and performance analysis of high-frequency transformer core materials. *Energies* **2023**, *16*, 3950. [CrossRef]
12. Stano, E.; Wiak, S. The accuracy of evaluation of the requirements of the standards IEC 61000-3-2 (12) with the application of the wideband current transducer. *Sensors* **2024**, *24*, 3693. [CrossRef] [PubMed]
13. Wu, B.; Zhou, H.; Lu, L. Research on error calibration technology of broadband voltage transformer. *Transformer* **2023**, *60*, 28–34.
14. Li, Z.; Lan, F.; Zhong, Y. Measurement-protection-integrated current sensor based on double-bobbin co-winding Technology. *High Volt. Technol.* **2022**, *48*, 4427–4436.
15. Liu, G.; Qin, Y.; Jang, C. Research on value traceability method of 500 kv standard voltage transformer. *Shandong Electr. Power* **2021**, *48*, 39–43.
16. Ge, Z.; Li, P.; Ren, D. Research on the traceability method of 1000 kV standard voltage transformers. *Ind. Meas.* **2021**, *31*, 8–11+14.
17. Yu, L.; Kai, L.; Jian, L.; Yi, C.; Chun, J. Analysis on measurement error of electromagnetic voltage transformer in frequency domain. *Electr. Meas. Instrum.* **2016**, *53*, 50–56.
18. Li, R.; Li, H.; Bi, J.; Yi, J.; Chen, J.; Jin, Y. Analysis of error characteristics of standard voltage transformers under low frequency conditions. *High Volt. Technol.* **2023**, *49*, 3719–3729.
19. Lei, M.; Jiang, C.; Li, D. Review of high voltage ratio standard devices technology. *High Volt. Eng.* **2021**, *47*, 1893–1904.
20. Wen, X.; Hu, G.; Yang, M. Wideband voltage measurement method of instrument transformer using edge computing. *High Volt. Eng.* **2022**, *48*, 1644–1652.
21. Nasiri-Zarandi, R.; Mirsalim, M. Finite-element analysis of an axial flux hysteresis motor based on a complex permeability concept considering the saturation of the hysteresis loop. *IEEE Trans. Ind. Appl.* **2015**, *52*, 1390–1397.
22. Ma, S.; Geng, H.; Liu, L.; Yang, G.; Pal, B.C. Grid-synchronization stability improvement of large scale wind farm during severe grid fault. *IEEE Trans. Power Syst.* **2017**, *33*, 216–226. [CrossRef]
23. Mitchell, S.D.; Welsh, J.S. The influence of complex permeability on the broadband frequency response of a power transformer. *IEEE Trans. Power Deliv.* **2009**, *25*, 803–813. [CrossRef]
24. Ren, Z.; Li, H.; Chen, X.; Yu, W.; Chen, R. Impedance modeling of self-inductive displacement sensor considering iron core reluctance and flux leakage. *IEEE Sens. J.* **2022**, *22*, 8583–8595. [CrossRef]
25. Kharezy, M.; Eslamian, M.; Thiringer, T. Estimation of the winding losses of medium frequency transformers with litz wire using an equivalent permeability and conductivity method. In Proceedings of the 2020 22nd European Conference on Power Electronics and Applications (EPE'20 ECCE Europe), Lyon, France, 7–11 September 2020; pp. P.1–P.7.

26. Zhang, C.; Han, Q. Frequency-depended modeling for the core of power transformer based on complex permeability considering interlaminar effects. *High Volt. Technol.* **2019**, *45*, 2292–2298.
27. Lin, Z. *High Voltage Instrument Transformers Technical Manual*; China Electric Power Press: Beijing, China, 2005.
28. Zhou, F. Research on Key Technologies of Harmonic Voltage Ratio Standard. Ph.D. Thesis, Huazhong University of Science and Technology, Wuhan, China, 2019.
29. Zhou, F.; Yin, X.; Jiang, C. Method to determine the errors voltage coefficient of standard voltage instrument transformer with high accuracy. *Proc. CSEE* **2019**, *39*, 7421–74828.
30. Kui, L.; Chenyu, X.; Feng, N.; Zijian, X.; Chaoran, W.; Yi, W. Modeling of residual current transformer considering nonlinear characteristics and design of output conditioning circuit parameters. *Proc. CSEE* **2022**, *42*, 3815–3826.

Disclaimer/Publisher's Note: The statements, opinions and data contained in all publications are solely those of the individual author(s) and contributor(s) and not of MDPI and/or the editor(s). MDPI and/or the editor(s) disclaim responsibility for any injury to people or property resulting from any ideas, methods, instructions or products referred to in the content.